Highly sensitive reduced graphene oxide microelectrode array sensor

Andrew M.H. Ng, Kenry, Chwee Teck Lim, Hong Yee Low, Kian Ping Loh

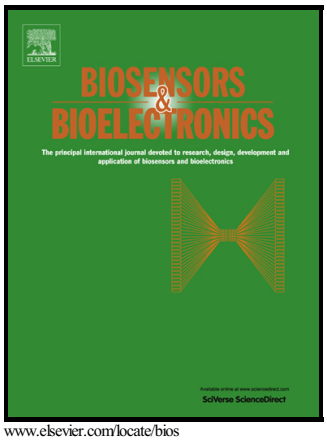

www.elsevier.com/locate/bios

PII: S0956-5663(14)00847-1
DOI: http://dx.doi.org/10.1016/j.bios.2014.10.048
Reference: BIOS7232

To appear in: *Biosensors and Bioelectronic*

Received date: 11 August 2014
Revised date: 6 October 2014
Accepted date: 20 October 2014

Cite this article as: Andrew M.H. Ng, Kenry, Chwee Teck Lim, Hong Yee Low and Kian Ping Loh, Highly sensitive reduced graphene oxide microelectrode array sensor, *Biosensors and Bioelectronic,* http://dx.doi.org/10.1016/j.bios.2014.10.048

Highly Sensitive Reduced Graphene Oxide Microelectrode Array Sensor

Andrew M. H. Ng[a,b], *Kenry*[b,c,d], *Chwee Teck Lim*[b,d,e], *Hong Yee Low*[a,f*], *Kian Ping Loh*[b*]

[a]Institute of Materials Research and Engineering, A*STAR (Agency for Science, Technology and Research), 3 Research Link, Singapore 117602

[b]Graphene Research Centre, Department of Chemistry, National University of Singapore, 3 Science Drive 3, Singapore 117543

[c]NUS Graduate School for Integrative Sciences and Engineering, National University of Singapore, Singapore 117576

[d]Department of Biomedical Engineering, National University of Singapore, Singapore 117576

[e]Mechanobiology Institute, National University of Singapore, Singapore 117411

[f]Engineering Product Development, Singapore University of Technology and Design, 20, Dover Drive, Singapore 138682

*Corresponding author. Tel: +65 6516 4402. E-mail Address: chmlohkp@nus.edu.sg (Kian Ping Loh)

Tel: +65 6499 4612. E-mail address: hongyee_low@sutd.edu.sg (Hong Yee Low)

Abstract: Reduced graphene oxide (rGO) has been fabricated into a microelectrode array (MEA) using a modified nanoimprint lithography (NIL) technique. Through a modified NIL process, the rGO MEA was fabricated by a self-alignment of conducting Indium Tin Oxide (ITO) and rGO layer without etching of the rGO layer. The rGO MEA consists of an array of 10 μm circular disks and microelectrode signature has been found at a pitch spacing of 60 μm. The rGO MEA shows a sensitivity of 1.91 nA μm^{-1} to dopamine (DA) without the use of mediators or functionalization of the reduced graphene oxide (rGO) active layer. The performance of rGO MEA remains stable when tested under highly resistive media using a continuous flow set up, as well as when subjecting it to mechanical stress.. The successful demonstration of NIL for fabricating rGO microelectrodes on flexible substrate presents a route for the large scale fabrication of highly sensitive, flexible and thin biosensing platform.

Keywords: Graphene; Microelectrode array; Biosensor; Nanoimprinting.

1. Introduction

A microelectrode has many advantages which include enhanced signal to noise ratios, increased mass diffusion, ease of miniaturization and operation in highly resistive media (Huang et al., 2009; Montenegro et al., 1991). However one of the disadvantages of reducing electrode sizes to sub-millimeter length scales is the reduced signals associated with the reduction in active area, where the current levels are reduced to nano and pico amp ranges. A commonly reported approach to enhance the signals is to functionalize the active layer with nanoparticles (Stern et al., 2006; Walcarius et al., 2013). Another method is to fabricate the sensor device into an array to allow an increase in total effective active area, thereby increasing the sensitivity of the sensor (Montenegro et al., 1991). In such an approach, the spacing between each microelectrode should be optimized so that the boundary layer of each microelectrode where concentration of the analyte differs from the concentration in bulk solution, also known as a diffusion hemisphere, do not overlap (Bard and Faulkner, 2000), as the latter occurrence will compromise the fast radial diffusion characteristics of an MEA (Henstridge and Compton, 2012; Tomčík, 2013).

In sensors, besides the electrode, the other critical component is the material that allows electrochemical reactions to occur – the active layer. Conventionally, gold, platinum and silver metals have been the predominant material used since the active layer needs to be electrically conductive (Finklea et al., 1993; Jung and Wilson, 1996; Lian et al., 2009; Lupu et al., 2009; Reed and Hawkridge, 1987). However there are other emerging organic electro-active materials such as poly(ethylenedioxythiophene), glassy carbon electrodes, carbon nanotubes, graphene, and reduced graphene oxide (rGO) (Chopra et al., 2003; Hsiao et al., 2013; Huang et al., 2013; Pron et al., 2010; Yuan and Shi, 2013). These materials are generally lower in cost to use and potentially allow for more useful fabrication techniques in contrast to conventional metal

sputtering/lithography methods, generating research interest in utilizing them in electrochemical applications (Forrest and Thompson, 2007).

There are several advantages of using rGO as an active layer in sensing applications. rGO is prepared by the chemical or thermal reduction of GO. Following the reduction process, oxygen atoms are partially removed from the surface and the sp^2 conjugation is recovered to some extent, thus allowing the rGO layer to be electrically conductive (Chua and Pumera, 2013). When used as an electrode, rGO can oxidise or reduce the target analyte depending on the analytes formal potential. rGO is has a large electrochemical potential window, easily solution processable, has oxygen moieties strewn across its carbon lattice that allow electrochemical reactions to take place. These attributes have been extensively covered in literature (Cai et al., 2014; Chen et al., 2013; W. Li et al., 2011; Ng et al., 2014; Penmatsa et al., 2012; Wei et al., 2012). Most previous studies focused on planar, macroscopic electrodes made of drop-casted or spin-coated rGO multilayer films onto pre-fabricated electrode platforms such as a glassy carbon electrode (GCE) (Saby et al., 1997; Wang et al., 2002). The solution processable nature of rGO allows it to be readily functionalized, creating an active material that can be highly tuned to specific analytes ranging from proteins, DNA and enzymes. Further in-depth reading into the detection properties of rGO has been published in the review article by Wu et al (Wu et al., 2013). However, addressing the problems of MEA fabrication of thin film active layers on rGO has been scarce due to the difficulties in integrating these into MEA configurations. One method to increase the currents is to fabricate the microelectrodes into an array format. In an array configuration with multiple microelectrode openings, these active layers work in parallel to increase the overall current in the sensor. However conventional microelectrode array fabrication methods have been developed mainly for thick metal active layers (Frazier, A.B. et

al., 1993), and the fabrication challenges for rGO MEAs arise from the difficulty in controlling the depth of etching for thin 2-D materials like rGO.

Li. F. et al previously reported a rGO MEA based on coating a substrate with a GO layer and using hydrazine filled polydimethylsiloxane (PDMS) wells to generate a spatial array of electrochemically active rGO disks. However one drawback with this method is that the initially insulating GO layer becomes electrochemically active due to inevitable electrochemical reduction during actual usage, which will lead to a loss of well-defined electrochemically active areas on the surface (F. Li et al., 2011). He. Q. et al reported patterning micron-size wide bands of GO using capillary actions through a PDMS stamp followed by its chemical reduction (He et al., 2010). However, this method is limited in terms of the shape and size of the rGO layers.

NIL is a method to create micro to nano scale surface patterns using thermal or UV curable resists. It is a mechanical replication process where the negative of the relief structure on a mold (typically Si or quartz) is transferred to a resist either at elevated temperature or under the exposure of UV radiation. The pattern resolution in NIL is governed primarily by the pattern resolution of the mold, and the imprint fidelity is mainly dependent on material properties and process optimization. NIL allows patterning of surfaces on a large scale with the patterned area only limited by the size of the mold. Most importantly, NIL is a versatile lithographic technique where various resists materials can be used and the imprint process window is tuneable according to the material properties. NIL presents a suitable fabrication method to create micro-array patterns (Chou et al., 1996; Guo, 2007). Through a process modification, we have recently reported the fabrication of size and shape tunable graphene and graphene oxide (Ng et al., 2014). Building on the earlier process development, here we report the fabrication of a biosensor based on microelectrode array of rGO and shows that these can function as highly sensitive biosensors.

2. Materials and Methods

All chemicals were purchased at Sigma-Aldrich unless otherwise stated.

2.1 GO Preparation

GO was produced by adding 1.5 g of Graphite powder, 1.5 g of $NaNO_3$ and 69 ml H_2SO_4 into a conical flask and stirred in an ice bath. 9 g of $KMnO_4$ was slowly added to the mixture which was cooled in the ice bath. Solution was then transferred to an oil bath at 35 ^oC. 120 ml of deionized (DI) water was added to the flask. Further stirring for 30 minutes as temperature of oil bath increased to 90 ^oC. 300ml of water was slowly added. 9 ml of H_2O_2 was added to the mixture. The solution was then filtered and washed through with DI water, leaving GO powder.

2.2 rGO MEA Device Fabrication

10% Polyvinylalcohol (PVA) was spin coated on rGO at 3000 rpm for 30 seconds. An Obducat nanoimprinter was used to imprint PVA at 105 ^oC, 50 bar for 10 minutes. The imprinted PVA layer was then etched using an Oxford RIE using 10 sccm of O_2 for 8 minutes. 1 µm thick Poly methylmethacrylate (PMMA) from Microresist Technology was then spin coated on top of the patterned and etched PVA layer at 3000 rpm for 30 seconds. The PMMA layer was then etched in an Oxford RIE using 10 sccm of O_2 for 5 minutes. The exposed PVA layer was then dissolved in DI water for 2 hours.

2.3 Electrochemical Reduction of GO

After spincoating GO onto the an Indium Tin Oxide/Polyethylene Terephthalate (ITO/PET), the GO layer was reduced by immersing the GO/ITO/PET substrate in 0.1 M Sodium phosphate buffer solution (Na-PBS) pH 4.5. The device was then held at -0.9 V for 3 minutes.

2.4 Electrochemical Experiments

Cyclic Voltammetry (CV), Differential Pulse Voltammetry (DPV) and Chronoamperometry (CA) were carried out using an Autolab potentiostat with a 3 electrode setup. A platinum mesh was used as the counter electrode and Ag/AgCl was used as the reference electrode.. Ruthenium (III) hexamine in 0.1 M KCl solution was used as the redox couple during CV.

DPV was conducted in 0.1 M Na-PBS (pH 7.4) solution with settings of 5 mV step potential, 25 mV modulation amplitude and 0.5 s interval time.

CA was conducted in 0.1 M Na-PBS (pH 7.4) solution with a constant potential of 0.5 V and 0.14 V and data acquisition of 0.05 s intervals for the interference experiment.

2.5 Microfluidic Device Fabrication

The microfluidic device has a width of 500 µm and a height of 100 µm and was designed using CAD software. The design was then fabricated in PDMS polymer (Sylgard 184, Dow Corning, USA) based on soft lithographic technique. In brief, the patterned SU-8-based silicon master was first silanized with trichloro(1H, 1H, 2H, 2H-perfluorooctyl)silane. Next, the PDMS pre-polymer was mixed with the curing agent, poured onto the silanized silicon wafer in a ratio of 10:1 (w/w) and subsequently cured at 80 ^{o}C for 2 hours. Holes of 1.5 mm were cored for fluidic inlets and

outlets. Finally, the PDMS mold was bonded to microscopic glass slide, with the rGO MEA sandwiched in between, using a homemade physical clamp.

3. Results and Discussion

In an earlier report, a sacrificial dual-resist NIL technique was developed to pattern chemical vapor deposited (CVD) graphene and graphene oxide (Ng et al., 2014). This technique allows us to pattern the molecular-thin graphene and graphene-oxide without needing an etching step, hence it offers the advantage of preserving the quality of the CVD grown graphene. Based on the same working principle, the NIL technique is used in this work as it further offers the advantage in the ease of tuning the microelectrode geometry and array density. One can tune the microelectrode pitch sizes to create a pattern array geometry that exhibits microelectrode behavior while maximizing the number of microelectrode openings.

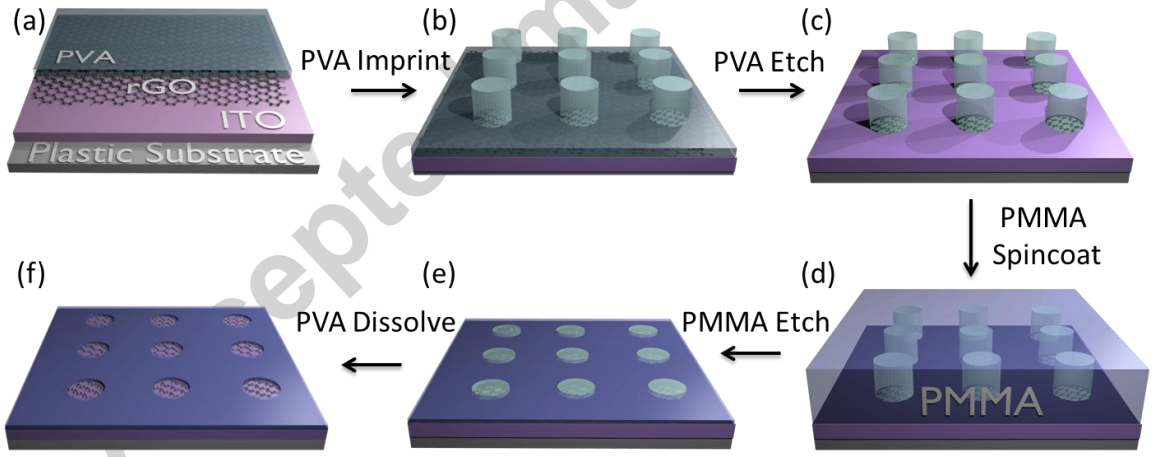

Figure 1. (a) PVA is spin coated onto electrochemically reduced graphene oxide (rGO). (b) PVA layer is patterned into a pillar array through NIL. (c) Patterned PVA layer is etched down to remove unwanted rGO, leaving PVA pillars protecting the rGO active layer array. (d) PMMA layer is spin-coated on top of the patterned and etched PVA layer. (e) PMMA layer etched to

expose PVA layer. (f) PVA layer is dissolved in DI water to reveal underlying rGO active layer. The final product consists of exposed rGO disk array surrounded by PMMA, the latter passivates the unexposed area from the electrolyte.

Figure 1 shows the fabrication process for the rGO MEAs. GO is spin coated onto ITO/PET substrate and electrochemically reduced using 0.1 M Na-PBS pH4.5 at -0.9 V for 3 minutes. GO is an insulating material, due to the oxidation process disrupting the sp^2 network. GO can be readily reduced using electrochemical reduction (see XPS data in Figure s1. showing reduction in oxygen-related signals). This results in a partial recovery of the π conjugation that is needed for electrical conduction (Chua and Pumera, 2013; Toh et al., 2014). A layer of PVA is then spin coated on top of the rGO layer (Figure 1a) and imprinted to create pillars of 10 μm in diameter over the surface of the rGO (Figure 1b). The patterned PVA layer functions as a sacrificial layer during the etching step, affording protection to the rGO layer below the pillars (Figure 1c). A layer of PMMA is then spin coated on top of the patterned PVA layer to act as the insulating barrier between the ITO and the electrolyte (Figure 1d). This step effectively eliminates the need to align the ITO with the rGO pattern array. Using two resists of differing soluble properties thus allows for a self-aligning mechanism to insulate the underlying ITO.

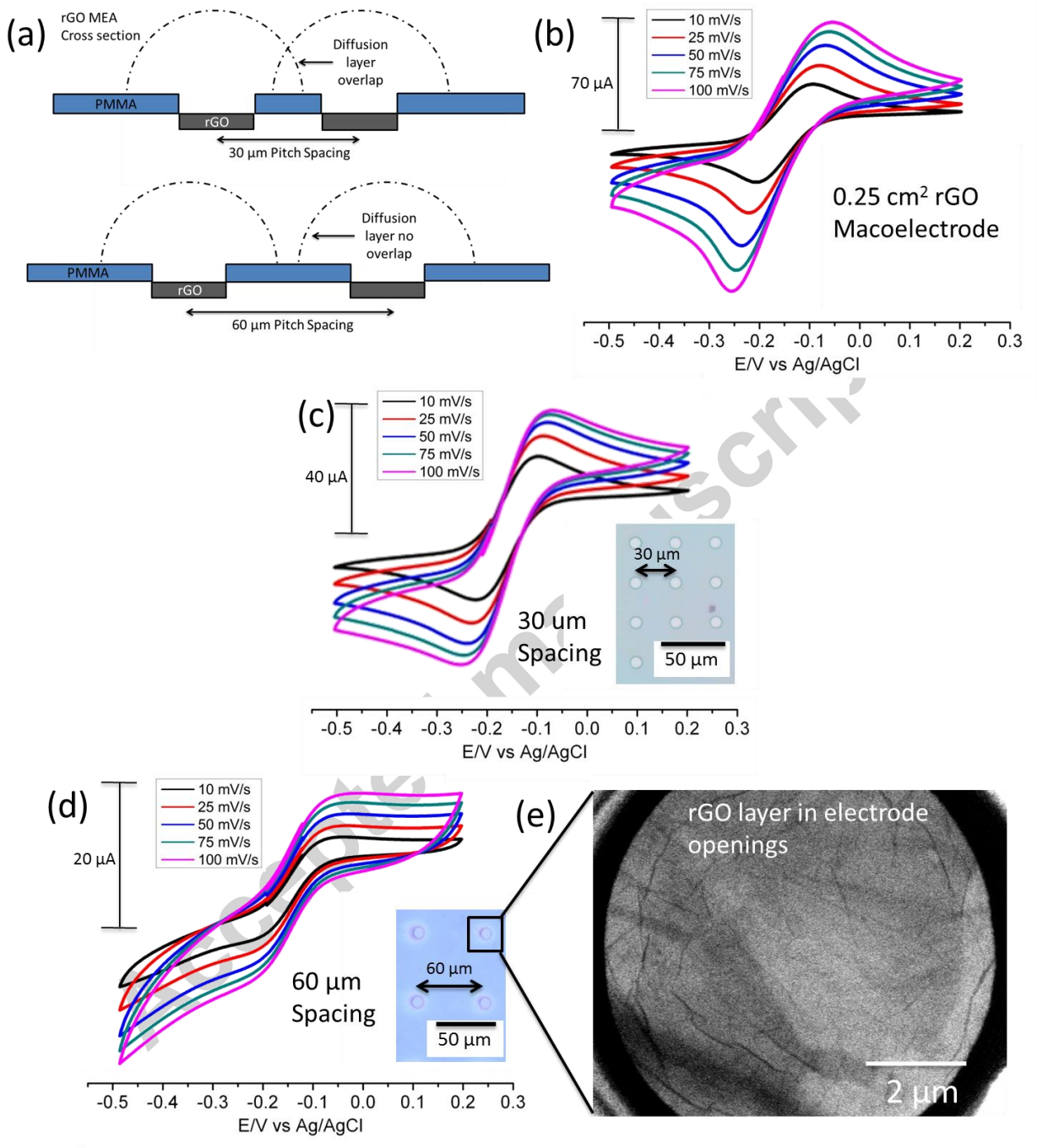

Figure 2. (a) Schematic of diffusion hemisphere overlapping when microelectrodes are fabricated in close proximity and no overlapping of diffusion hemispheres when microelectrodes are fabricated at pitch distances greater than twice the radius of the diffusion hemisphere. (b) CV data with increasing scan rate, using a 0.25 cm^2 rGO macroelectrode. (c) CV data of rGO MEA

with 30 µm pitch spacing. (d) CV data of rGO MEA with 60 µm pitch spacing. (e) SEM image of rGO layer inside an exposed microelectrode.

The fabricated rGO MEA consists of an array of 10 µm disks separated by various pitch spacing. CV characterization was done using 2.5 mM ruthenium hexamine as the redox probe to determine the minimum pitch spacing between the individual microelectrodes which allows microelectrode behavior. Figure 2a shows the schematic of how the MEA geometry can affect the overlap of diffusion hemispheres and cause the device to function as a macroelectrode instead of a microelectrode. Pitch distances between microelectrodes are required to be greater than two times the radius of the diffusion hemisphere in order for the diffusion layers to be non-overlapping. Using an equation to determine the diffusion layer thickness (Tomčík, 2013), we calculate the diffusion hemisphere radius to be approximately 27 µm at a scan rate of 10 mV/s. Figure 2b shows a rGO macroelectrode with classical peak shaped CV behavior; as can be seen in Figures 2c and 2d, when the pitch spacing is increased from 30 to 60 µm, the depletion zone in the CV reduces and a classic sigmoidal shaped CV emerges as the sensors transit from macroelectrode to microelectrode behavior. At a spacing of 60 µm, the diffusion hemispheres of the individual microelectrodes cease to overlap as evidenced by the sigmoidal CV shape in Figure 2d. This agrees with the calculation of the diffusion hemisphere radius being 27 µm. As long as the geometry for the rGO MEA has a pitch spacing larger than twice the diffusion layer radius, the device would operate in a microelectrode array regime. Subsequently all rGO MEAs were fabricated using 60 µm pitch spacings. Figure 2e shows an SEM image of the rGO active layer within a microelectrode as evidenced by the slight wrinkles that is characteristic of rGO. The image shows that rGO flakes remain stable within the microelectrode openings with no signs of lift off or peeling during electrochemical analysis.

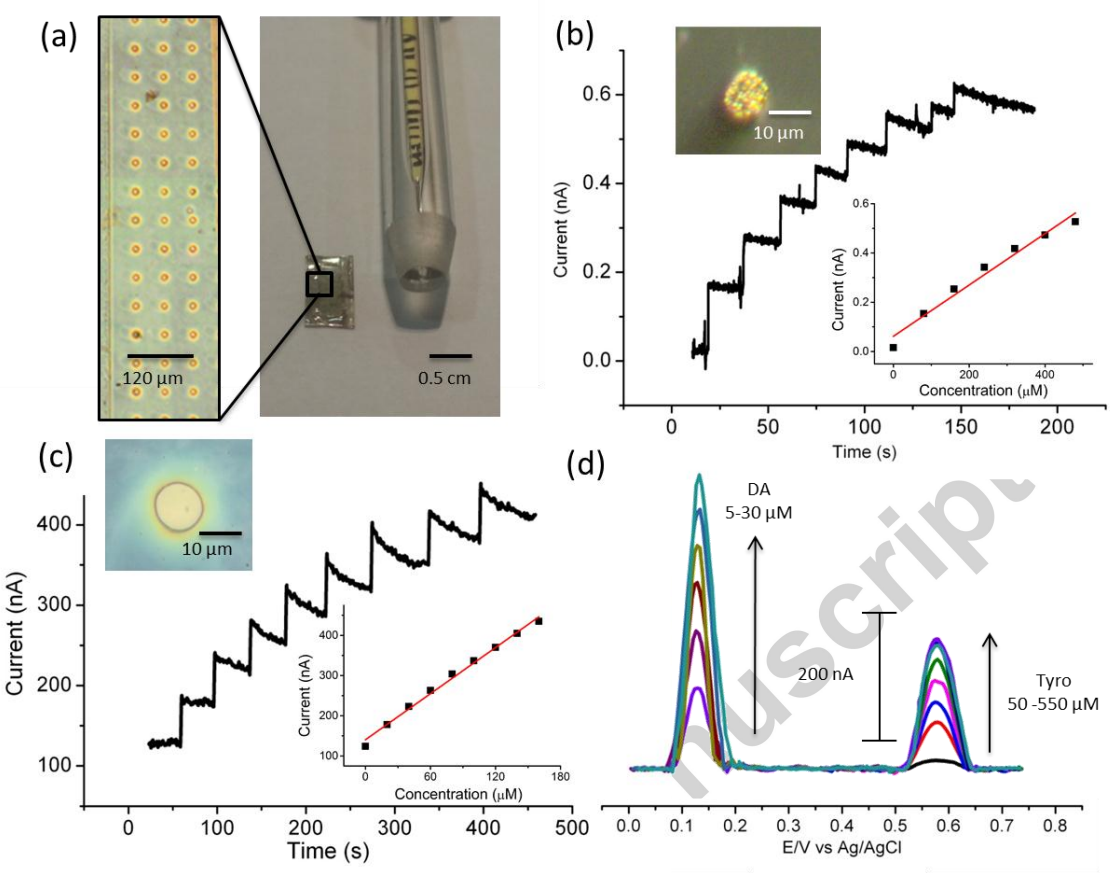

Figure 3. (a) Comparison of rGO MEA and Au microelectrode. Inset shows surface of rGO MEA with 10 µm microelectrode holes. (b) CA of Au microelectrode towards 100 µM injections of DA. Top inset shows image of gold active layer, bottom inset shows calibration graph. (c) CA of rGO MEA towards 20 µM injections of DA. Top inset shows single microelectrode and bottom inset shows calibration graph. (d) Simultaneous detection of DA and Tyrosine (Tyro) using DPV.

The electrochemical performance of a commercially available gold microelectrode (Metrohm) (Figure 3a) was compared to the rGO MEA device, using DA as the analyte. Irregular concentrations of DA, a neurotransmitter, is related to Parkinson's disease and attention deficit hyperactivity disorder and have been linked to other nervous system related diseases (Bernheimer et al., 1973; Contreras et al., 2002; Gj et al., 1996). DA has been extensively reported to be electrochemically active towards metal and carbon based sensors including rGO (Barnes et al., 2010; Gai et al., 2013; Hubbard et al., 1984; Yang-Rae Kim, 2010; Yu et al., 2014; Zachek et al., 2008; Zhu et al., 2013, 2012). At a potential of 0.14 V, DA undergoes a two electron-oxidation process, (one electron from each of its hydroxyl groups) (Colin-Orozco et al., 2012) to the resulting in an anodic current that is proportional to the concentration of DA in solution. Figure 3b shows CA response of the gold microelectrode towards 100 µM additions of DA, the gold microelectrode had a sensitivity of 0.001 nA μM^{-1} and a limit of detection of 3.6 µM (signal to noise ratio of 3). Figure 3c shows the CA response of the rGO MEA device towards addition of DA (20 µM). The rGO MEA device displays a sensitivity of 1.91 nA μM^{-1} with a detection limit of 0.26 µM (signal-to-noise ratio of 3).

The higher current signal in rGO MEA compared to gold microelectrode arises from the larger diffusion flux that is associated with the radial diffusion profile at its individual microelectrodes (Zoski, 2007). Using the CA data we determine the sensitivity of the rGO MEA device and compare its response to other graphene-based devices. From Table 1, it can be seen that the rGO MEA devices sensitivity is greater than other graphene based devices reported in the literature. We also note that the size of the active area is significantly smaller in our rGO MEA devices, and that no functionalization of the rGO layer has been performed, thus attesting to the fact that

inherent sensitivity can be maintained even when the size is scaled down due to the enhanced diffusion flux of analytes in MEA geometry.

Table 1. Comparison of sensitivities of electrodes towards DA detection

Sensor Type	Sensitivity (nA μM^{-1})	Active Area (mm^2)	Ref.
Glassy Carbon Electrode (GCE) with Copper Chloride Complex	2.02	7.1	(Sotomayor et al., 2003)
Ferrocene bound Nafion Membrane Electrode	1.1	7.1	(Kumar et al., 2010)
rGO with Gold Nanoparticles	0.0627	7.1	(Yang et al., 2012)
GCE with Carbon nanotubes/Chitosan Composite	0.328	7.1	(Babaei et al., 2011)
Gold Microelectrode	0.001	0.0000785	This work.
rGOMEA	1.91	0.017	This work.

Figure 3d shows simultaneous detection of Tyro and DA using DPV. Tyro is an amino precursor building block for DA. Simultaneous detection of DA and Tyro under physiological conditions could be potentially useful for diagnosis and health monitoring. We noticed that the oxidation potential of Tyro at 0.59 V as recorded on rGO MEA is lower than the values obtained by previously reported graphene-based Tyro detection methods (Wei et al., 2012; Xiaozhi Yu, 2008). The sensitivity of the rGO MEA devices towards DA and Tyro is 12.7 and 0.34 nA μM^{-1}

(Figure s2), with a detection limit of 0.1 µM and 3.7 µM (signal to noise ratio of 3), respectively. The rGO MEA was also used to detect hydrogen peroxide (Figure s3), where the device displays a sensitivity of 2.3 nA μM^{-1} with a detection limit of 0.35 µM (signal to noise ratio of 3).

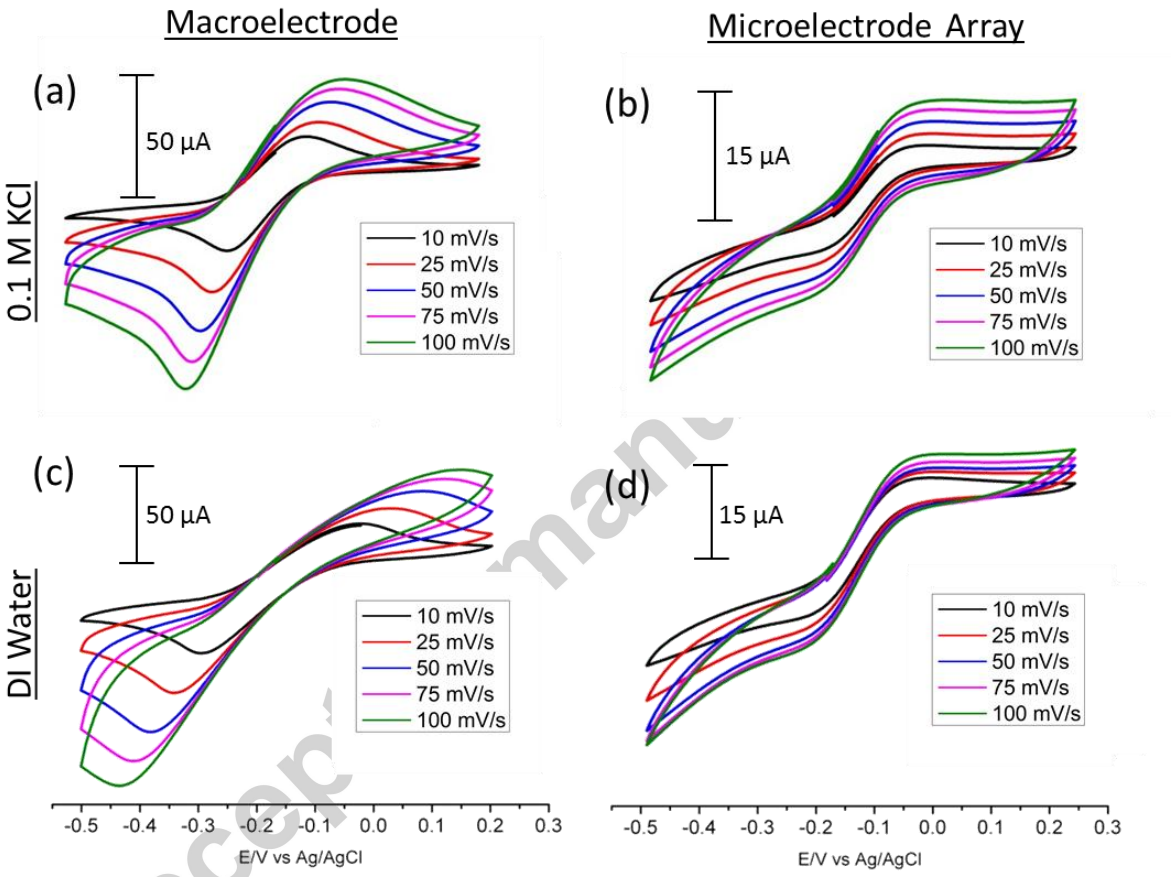

Figure 4. (a) CV of rGO macroelectrode in 0.1M KCl solution. (b) CV of rGO MEA in 0.1M KCl solution. (c) CV of rGO macroelectrode in DI water. (d) CV of rGO MEA in DI Water.

In physiological fluids, the solution conductivity is often low, thus it is important for a biosensor to retain its established electrocatalytic characteristics (sensitivities, point of oxidation/reduction) in these media. A 0.25 cm^2 rGO macroelectrode and rGO MEA device were comparatively

tested using ruthenium hexamine as the redox analyte in 0.1M KCl and deionized water, the latter have conductivity of 12.9 mS cm^{-1} and 55 nS cm^{-1}, respectively (Pashley et al., 2005; Pratt, 1991). As can be seen in Figure 4, the performance of the rGO MEA was largely unaffected in deionized water environments, the redox peaks for ruthenium hexamine occurs at -0.1V and -0.2V, respectively. As scan rates increase, the peak-to-peak separation remains constant. This is due to the low ohmic drop associated with microelectrodes (Aoki, 1993). In contrast, macroelectrodes experience ohmic drop in solutions of low conductivity as the potential at the active layer of a macrolectrode lags the applied potential, this can cause significant inaccuracies in analyte detection since larger voltage sweep ranges need to be applied to account for the ohmic drop. Ohmic drop can be clearly seen in the increasing peak-to-peak separation distances in Figure 4c for the rGO macroelectrode in DI water. The peak-to-peak separation increases from 300 mV at 10 mV s^{-1} scan rate to 500 mV at a scan rate of 100 mV s^{-1}, which indicates extremely sluggish kinetics. In contrast, the peak-to-peak separation remains constant in rGO MEA with scan rate, thus the advantage of rGO MEAs is that it can operate robustly in electrolytes having conductivity differences of nearly 6 orders of magnitude.

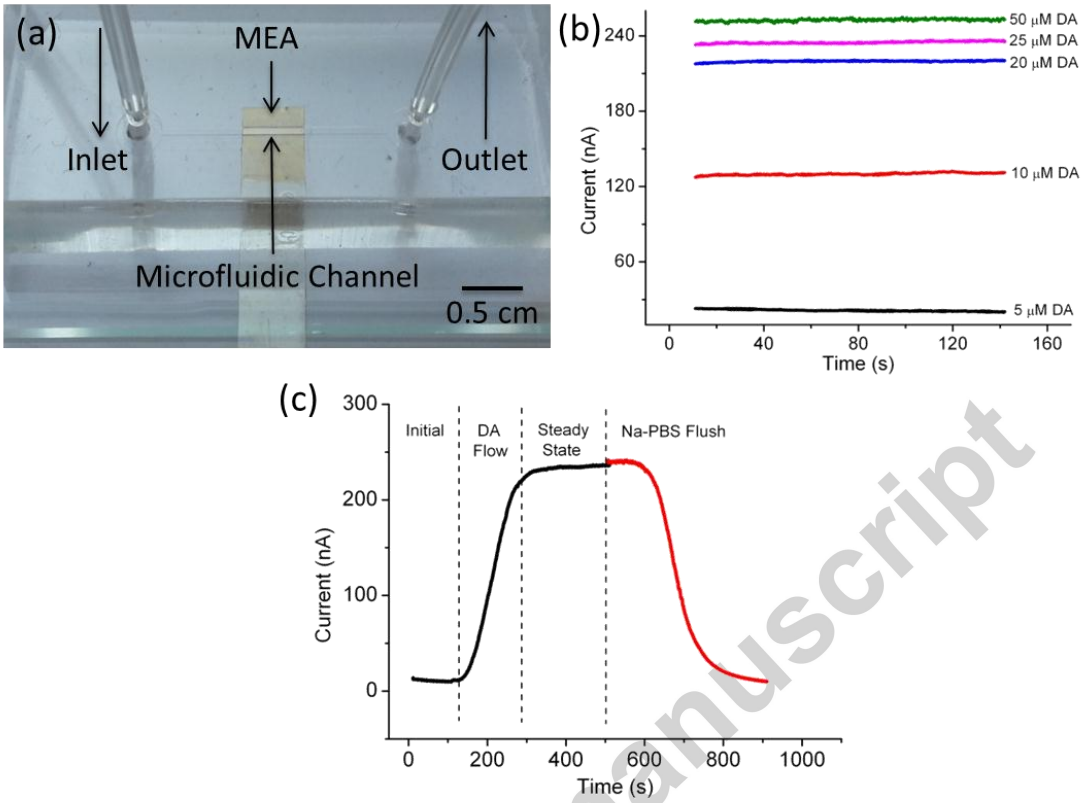

Figure 5. (a) Image of the rGO MEA device in the microfluidic system. (b) Steady state currents for differing concentrations of DA pumping through the microfluidic channel. (c) Example of CA response to the flowing of 25 μM DA and flushing with pure Na-PBS.

It has been reported that the operation of MEAs are relatively independent of solution flows (Fungaro and Brett, 1999). The flat planar shape of the rGO MEA devices allows it to be readily integrated into a simple microfluidic system (Figure 5a) with a channel width of 500 μm and height of 100 μm. Solutions of 0.1M Na-PBS with differing concentrations of DA from 5 to 50 μM were injected into the channel and Figure 5b shows the steady state current response using CA. Figure 5c shows the signal response when DA flows through the system. Flowing pure Na-PBS through the channel gave a steady state current of approximately 10 nA. Once a 25 μM

DA stock solution flowed through the system, the steady state current increased to a value of 230 nA. After each run, the channel was flushed with pure NA-PBS solution. The red line depicts the signal returning to the baseline current once DA was flushed out. The highly reproducible flow sensing shows successful integration of the rGO MEA into a microfluidic system.

Fouling by biological solution is a common problem biosensors. When increasing concentrations of AA was added, the DPV peak shifted to higher onset potentials and the anodic current decreased, which is evidence of surface fouling. The device could be readily cleaned in 0.1M Na-PBS by holding it at 0.6V for 3 minutes. At this potential the AA fouling was removed as AA was oxidized to L-dihydroascorbic acid which readily diffused away from the electroactive regions. Figure s4 depicts the response of the cleaned device showing a similar response towards DA as compared to the pristine device before fouling.. This shows that the surface of the rGO electrode is relatively inert and only weak non-covalent bonding exists between biomolecules and the electrode surface.

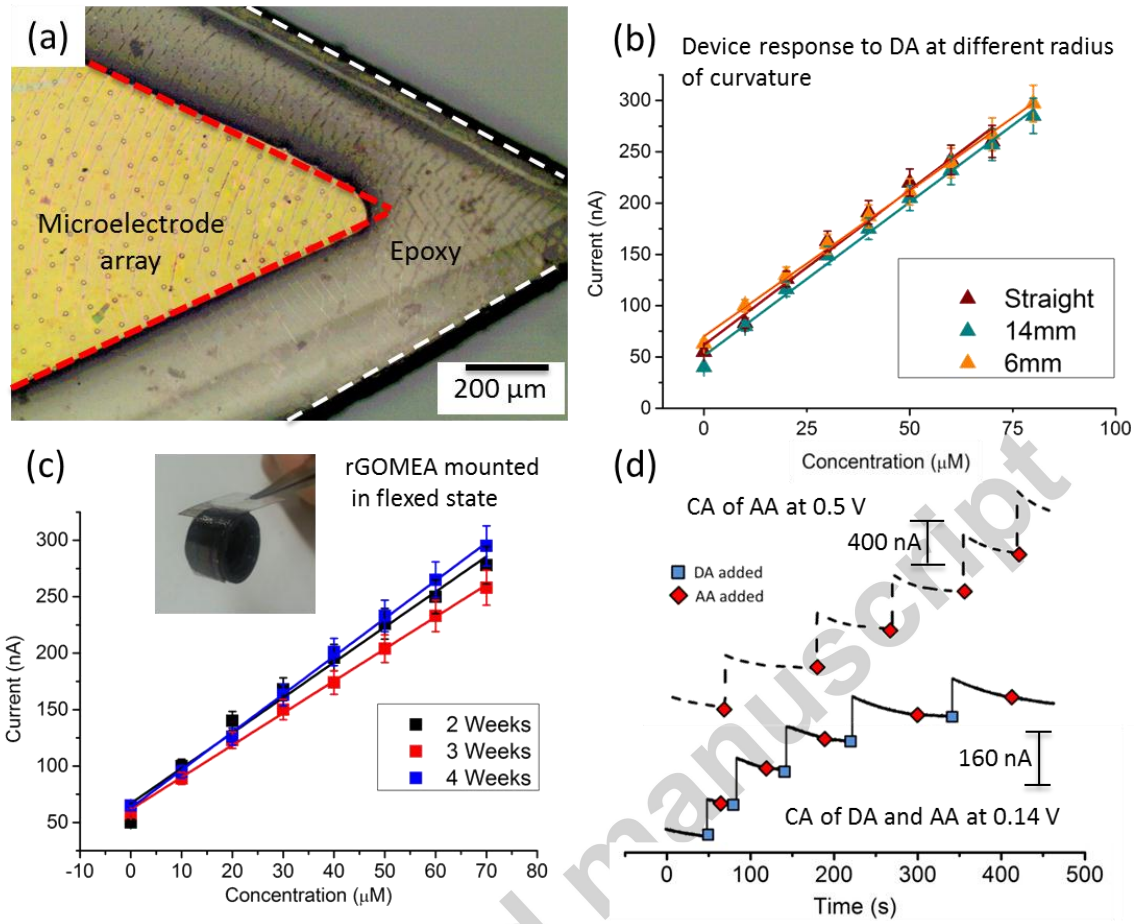

Figure 6. (a) rGO MEA device cut from ITO/PET substrate where it is fabricated on. (b) Comparison of rGO MEA performance towards DA when flexed at different radius of curvatures. (c) Flex tests of rGO MEA device over a span of 4 weeks, showing no change in device performance. (d) CA response graphs of rGO MEA device to AA at 0.5V (top) and DA in the presence of AA at 0.14V (bottom). At this potential the device shows selective response to DA.

The NIL fabrication process allows the microelectrode array to be fabricated across a large area on flexible substrates, after which any arbitrary size and shape of the devices active area can be cut from the original piece, this allows precise tailoring of the device dimensions to fit any given

environment (Figure 6a). The mechanical flexibility of rGO is promising for flexible electronics (Cong et al., 2013). The device performance in a flexed state towards DA detection was measured and compared to the performance in an unflexed state. The rGO MEA devices was mounted onto surfaces with radius of curvatures of 14 mm and 6 mm. The CA calibration graphs in Figure 6b shows negligible change in the device response to DA concentrations at increasing flex angles. To test the reliability of the sensor we measured the devices response in multiple sample runs (>15) using 10 μM DA injections and calculated the relative standard deviation to be 4.7%, which indicates good reliability (Mao et al., 2011; Sotomayor et al., 2003). In order to investigate if the rGO MEA remains operational when mechanically flexed, the rGO MEA was mounted on a curved surface of 6 mm radius of curvature (inset of Figure 6b) for an extended period of time. It was found that highly reproducible and stable current signals towards DA could be obtained from the device even after keeping the MEA in a continuous flexed state for 4 weeks (Figure 6c), showing that rGO is a suitable as an active layer for flexible sensor. This is attributed to the superior mechanical stability of rGO.

The rGO MEA electrode can also be operated in selective sensing mode. Figure 6d shows detection of DA with AA as an interferant. DA and AA have similar oxidizing potentials and could not be differentiated using DPV. However tuning the CA potential allows the selective detection of DA over AA. DA is more readily oxidized at the rGO surface due to its higher affinity to rGO arising from π-π stacking, as compared to AA which contains a pentene ring in its molecular structure (Gao et al., 2013). The top CA graph in Figure 6d shows the detection of AA by the device at higher voltages (0.5V). The bottom CA graph shows consecutive DA and AA injection into the system at a voltage that allows for DA oxidation but not AA (0.14 V). As shown, the current increases (70 nA) only when DA is injected into the system whereas the

increase in current when AA is injected is negligible (2 nA). Uric acid (UA) is also a common interferant however oxidation of UA only occurs at a higher potential (0.28 V) (Figure s5) in this case and therefore does not have any effect on DA detection when operated at a lowered potential of 0.14 V.

4. Conclusion

A microelectrode array sensor based on rGO has been successfully fabricated using NIL. The rGO MEA exhibits sigmoidal-shaped cyclic voltammetric response and high signal-to-noise ratio in the sensing of bioanalytes such as DA, Tyro and hydrogen peroxide. In the CA detection mode, rGO MEA exhibits a sensitivity of 1.91 nA μM^{-1} with a detection limit of 0.26 µM for DA and sensitivities of 2.3 nA μM^{-1} with a detection limit of 0.35 µM for hydrogen peroxide. Simultaneous detection of DA and Tyro using DPV yielded sensitivities of 12.7 and 0.34 nA μM^{-1}, with detection limits of 0.1 and 3.7 µM for DA and Tyro, respectively. The performance of the rGO MEAs is significantly higher than other macroscopic graphene electrodes in terms of sensitivity and tolerance for low conductivity electrolyte. Sensitivity was unaffected under a continuous flow condition when the rGO MEA was incorporated in a microfluidic device. Furthermore, the sensor shows remarkable mechanical stability and can be operated for an extended period of time in a flexed state.

5. References

Aoki, K., 1993. Electroanalysis 5, 627–639.

Babaei, A., Babazadeh, M., Momeni, H.R., 2011. Int J Electrochem Sci 6, 1382–1395.

Bard, A.J., Faulkner, L.R., 2000. Electrochemical Methods: Fundamentals and Applications. Wiley, New York.

Barnes, E.O., O'Mahony, A.M., Aldous, L., Hardacre, C., Compton, R.G., 2010. J. Electroanal. Chem. 646, 11–17.

Bernheimer, H., Birkmayer, W., Hornykiewicz, O., Jellinger, K., Seitelberger, F., 1973. J. Neurol. Sci. 20, 415–455.

Cai, B., Wang, S., Huang, L., Ning, Y., Zhang, Z., Zhang, G.-J., 2014. ACS Nano 8, 2632–2638.

Chen, N., Li, X., Wang, X., Yu, J., Wang, J., Tang, Z., Akbar, S.A., 2013. Sens. Actuators B Chem. 188, 902–908.

Chopra, S., McGuire, K., Gothard, N., Rao, A.M., Pham, A., 2003. Appl. Phys. Lett. 83, 2280–2282.

Chou, S.Y., Krauss, P.R., Renstrom, P.J., 1996. J. Vac. Sci. Technol. B 14, 4129–4133.

Chua, C.K., Pumera, M., 2013. Chem. Soc. Rev. 43, 291–312.

Colin-Orozco, E., Corona-Avendano, S., Ramirez-Silva, M.T., Romero-Romo, M., Palomar-Pardave, M., 2012. Int. J. Electrochem. Sci. 7, 6097–6105.

Cong, H.-P., Ren, X.-C., Wang, P., Yu, S.-H., 2013. Energy Environ. Sci. 6, 1185–1191.

Contreras, F., Fouillioux, C., Bolívar, A., Simonovis, N., Hernandez, R., Hernandez, M.J., Lezama, E., Velasco, M., 2002. Int. Congr. Ser., Current trends in clinical medicine 1237, 99–107.

Finklea, H.O., Snider, D.A., Fedyk, J., Sabatani, E., Gafni, Y., Rubinstein, I., 1993. Langmuir 9, 3660–3667.

Forrest, S.R., Thompson, M.E., 2007. Chem. Rev. 107, 923–925.

Frazier, A.B., O'Brien, D.P., Allen, M.G., 1993. IEEE.

Fungaro, D.A., Brett, C.M.A., 1999. Anal. Chim. Acta 385, 257–264.

Gai, P., Zhang, H., Zhang, Y., Liu, W., Zhu, G., Zhang, X., Chen, J., 2013. J. Mater. Chem. B 1, 2742–2749.

Gao, F., Cai, X., Wang, X., Gao, C., Liu, S., Gao, F., Wang, Q., 2013. Sens. Actuators B Chem. 186, 380–387.

Gj, L., Jm, S., Sb, W., C, G., T, W., N, K., Jl, K., 1996. Mol. Psychiatry 1, 121–124.

Guo, L.J., 2007. Adv. Mater. 19, 495–513.

Henstridge, M.C., Compton, R.G., 2012. Chem. Rec. N. Y. N 12, 63–71.

He, Q., Sudibya, H.G., Yin, Z., Wu, S., Li, H., Boey, F., Huang, W., Chen, P., Zhang, H., 2010. ACS Nano 4, 3201–3208.

Hsiao, Y.-S., Kuo, C.-W., Chen, P., 2013. Adv. Funct. Mater. n/a–n/a.

Huang, K.-J., Wang, L., Li, J., Yu, M., Liu, Y.-M., 2013. Microchim. Acta 180, 751–757.

Huang, X.-J., O'Mahony, A.M., Compton, R.G., 2009. Small 5, 776–788.

Hubbard, A.T., Stickney, J.L., Soriaga, M.P., Chia, V.K.F., Rosasco, S.D., Schardt, B.C., Solomun, T., Song, D., White, J.H., Wieckohski, A., 1984. J. Electroanal. Chem. Interfacial Electrochem. 168, 43–66.

Jung, S.-K., Wilson, G.S., 1996. Anal. Chem. 68, 591–596.

Kumar, A.S., Swetha, P., Pillai, K.C., 2010. Anal. Methods 2, 1962.

Lian, W., Wang, L., Song, Y., Yuan, H., Zhao, S., Li, P., Chen, L., 2009. Electrochimica Acta 54, 4334–4339.

Li, F., Xue, M., Ma, X., Zhang, M., Cao, T., 2011. Anal. Chem. 83, 6426–6430.

Li, W., Geng, X., Guo, Y., Rong, J., Gong, Y., Wu, L., Zhang, X., Li, P., Xu, J., Cheng, G., Sun, M., Liu, L., 2011. ACS Nano 5, 6955–6961.

Lupu, S., Lete, C., Marin, M., Totir, N., Balaure, P.C., 2009. Electrochimica Acta 54, 1932–1938.

Mao, Y., Bao, Y., Gan, S., Li, F., Niu, L., 2011. Biosens. Bioelectron. 28, 291–297.

McAlpine, M.C., Ahmad, H., Wang, D., Heath, J.R., 2007. Nat. Mater. 6, 379–384.

Montenegro, M.I., Montenegro, I., Queirós, M.A., Daschbach, J.L., 1991. Microelectrodes: Theory and Applications: Theory and Applications. Kluwer Academic Publishers, The Netherlands.

Ng, A.M.H., Wang, Y., Lee, W.C., Lim, C.T., Loh, K.P., Low, H.Y., 2014. Carbon 67, 390–397.

Pashley, R.M., Rzechowicz, M., Pashley, L.R., Francis, M.J., 2005. J. Phys. Chem. B 109, 1231–1238.

Penmatsa, V., Kim, T., Beidaghi, M., Kawarada, H., Gu, L., Wang, Z., Wang, C., 2012. Nanoscale 4, 3673.

Pratt, K.W., 1991. J Res Natl Inst Stand Technol 96, 191.

Pron, A., Gawrys, P., Zagorska, M., Djurado, D., Demadrille, R., 2010. Chem. Soc. Rev. 39, 2577.

Reed, D.E., Hawkridge, F.M., 1987. Anal. Chem. 59, 2334–2339.

Saby, C., Ortiz, B., Champagne, G.Y., Bélanger, D., 1997. Langmuir 13, 6805–6813.

Sotomayor, M.D.P.T., Tanaka, A.A., Kubota, L.T., 2003. Electroanalysis 15, 787–796.

Stern, E., Jay, S., Bertram, J., Boese, B., Kretzschmar, I., Turner-Evans, D., Dietz, C., LaVan, D.A., Malinski, T., Fahmy, T., Reed, M.A., 2006. Anal. Chem. 78, 6340–6346.

Toh, S.Y., Loh, K.S., Kamarudin, S.K., Daud, W.R.W., 2014. Chem. Eng. J. 251, 422–434.

Tomčík, P., 2013. Sensors 13, 13659–13684.

Walcarius, A., Minteer, S.D., Wang, J., Lin, Y., Merkoçi, A., 2013. J. Mater. Chem. B 1, 4878–4908.

Wang, J., Li, M., Shi, Z., Li, N., Gu, Z., 2002. Electroanalysis 14, 225–230.

Wei, J., Qiu, J., Li, L., Ren, L., Zhang, X., Chaudhuri, J., Wang, S., 2012. Nanotechnology 23, 335707.

Wu, S., He, Q., Tan, C., Wang, Y., Zhang, H., 2013. Small 9, 1160–1172.

Xiaozhi Yu, Z.M., 2008. Electroanalysis 20, 1246 – 1251.

Yang, J., Strickler, J.R., Gunasekaran, S., 2012. Nanoscale 4, 4594–4602.

Yang-Rae Kim, S.B., 2010. Biosens. Bioelectron. 25, 2366–2369.

Yuan, W., Shi, G., 2013. J. Mater. Chem. A 1, 10078–10091.

Yu, X., Sheng, K., Shi, G., 2014. Analyst 139, 4525–4531.

Zachek, M.K., Hermans, A., Wightman, R.M., McCarty, G.S., 2008. J. Electroanal. Chem. Lausanne Switz. 614, 113–120.

Zhu, W., Chen, T., Ma, X., Ma, H., Chen, S., 2013. Colloids Surf. B Biointerfaces 111, 321–326.

Zhu, X., Liu, Q., Zhu, X., Li, C., Xu, M., Liang, Y., 2012. Int J Electrochem Sci 7, 5172–5184.

Zoski, C.G., 2007. Handbook of Electrochemistry. Elsevier, The Netherlands.

Highlights

Highly Sensitive Reduced Graphene Oxide Microelectrode Array Sensor

- We show a process to fabricate microelectrode array sensors for thin active layers.
- Process is used to fabricate reduced graphene oxide sensor on flexible plastic.
- The sensor displayed high sensitivities towards dopamine.
- The sensor performance was investigated in highly resistive media.
- The sensor was integrated into a microfluidic system.